Constraining the time variation of Newton's constant G with gravitational-wave standard sirens and supernovae

Wen Zhao[1,2], Bill S. Wright[3], Baojiu Li[4]

[1] *CAS Key Laboratory for Researches in Galaxies and Cosmology,*
Department of Astronomy, University of Science and Technology of China,
Chinese Academy of Sciences, Hefei, Anhui 230026, China
[2] *School of Astronomy and Space Science, University of Science and Technology of China, Hefei 230026, China*
[3] *Institute of Cosmology & Gravitation, University of Portsmouth, Portsmouth, Hampshire, PO1 3FX, UK*
[4] *Institute for Computational Cosmology, Department of Physics, Durham University, Durham DH1 3LE, UK*

The intrinsic peak luminosity of Type Ia supernovae (SNIa) depends on the value of Newton's gravitational constant G, through the Chandrasekhar mass $M_{\rm Ch} \propto G^{-3/2}$. If the luminosity distance can be independently determined, the SNIa can be treated as a tracker to constrain the possible time variation of G in different redshift ranges. The gravitational-wave (GW) standard sirens, caused by the coalescence of binary neutron stars, provide a model-independent way to measure the distance of GW events, which can be used to determine the luminosity distances of SNIa by interpolation, provided the GW and SNIa samples have similar redshift ranges. We demonstrate that combining the GW observations of third-generation detectors with SNIa data provides a powerful and model-independent way to measure G in a wide redshift range, which can constrain the ratio G/G_0, where G and G_0 are respectively the values in the redshift ranges $z > 0.1$ and $z < 0.1$, at the level of 1.5%.

I. INTRODUCTION

The measurement of Newton's constant G is one of the key tasks in modern physics. In General Relativity, G is assumed to be constant. However, in general alternative theories of gravity, it can become both time- and space-dependent. For instance, in Brans-Dicke gravity, the value of G is inversely proportional to the mean value of the scalar field ϕ in the Universe, which evolves with the expansion of the Universe [1]. While in general screened modified gravity, which is a kind of scalar-tensor theory with screening mechanisms, the value of G depends both on the mean value of the scalar field ϕ in the Universe and on the local Newtonian potential of the observed object [2]. Numerous methods have been proposed to measure G on different time scales, including the lunar ranging experiment [3], pulsar timing observations [4], Big Bang nucleosynthesis (BBN) observations [5] and so on [6, 7].

Type Ia supernovae (SNIa) are 'standard candles' in the standard cosmological model [8]. However, analytical models of their light curves generally predict that the absolute magnitude of a SNIa depends on the value of G. Therefore, measuring the absolute magnitude of SNIa can determine the values of G at different redshifts. To achieve this, the luminosity distance $d_{\rm L}$ to each SNIa should be independently determined, which is requisite to fix the absolute magnitude of SNIa from observations. In previous works [9, 10], the independent determination of $d_{\rm L}$ is given by assuming specific cosmological models. For instance, in [9] the authors determined the distance $d_{\rm L}$ of SNIa by assuming a flat universe without cosmological constant but with a varying G as a function of redshift. While in [10], the authors assumed the ΛCDM model, or a polynomial form of the Hubble parameter. These assumptions induce that the resulting constraints on G in these papers are model-dependent. We avoid this issue by considering the potential observations of GW standard sirens in similar redshift ranges to those of the SNIa, which provide the desired independent measurement of $d_{\rm L}$ [1]. Therefore, combining SNIa and GW data provides a novel way to measure G on a cosmological scale. In this method, the constraint on G is at the time of the SNIa. Thus, once a sufficient number of events have been observed, a constraint map, as a function of redshift, could be constructed.

II. GRAVITATIONAL DEPENDENCE OF SNIA

The empirical observation of SNIa gives the distance estimation, under the assumption that all SNIa have the same intrinsic luminosity if they are identical in colour, shape and galactic environment [13]. This model expresses the distance modulus in an isotropic universe, $\mu = 5 \log_{10}(d_{\rm L}/10{\rm pc})$, as

$$\mu = m_{\rm B}^* - (M_{\rm B} - \alpha \times X_1 + \beta \times C), \tag{1}$$

---

[1] In addition to the GW standard sirens, the Cepheid variables can also be used to measure the distance $d_{\rm L}$ of SNIa, if we assume their empirical period-luminosity relation [11]. However, this measurement suffers from two defects: First, only the nearby Cepheid variables are observable, so this method is applicable only for extremely low-redshift range. Second, this method depends on the so-called cosmic distance ladder [12].
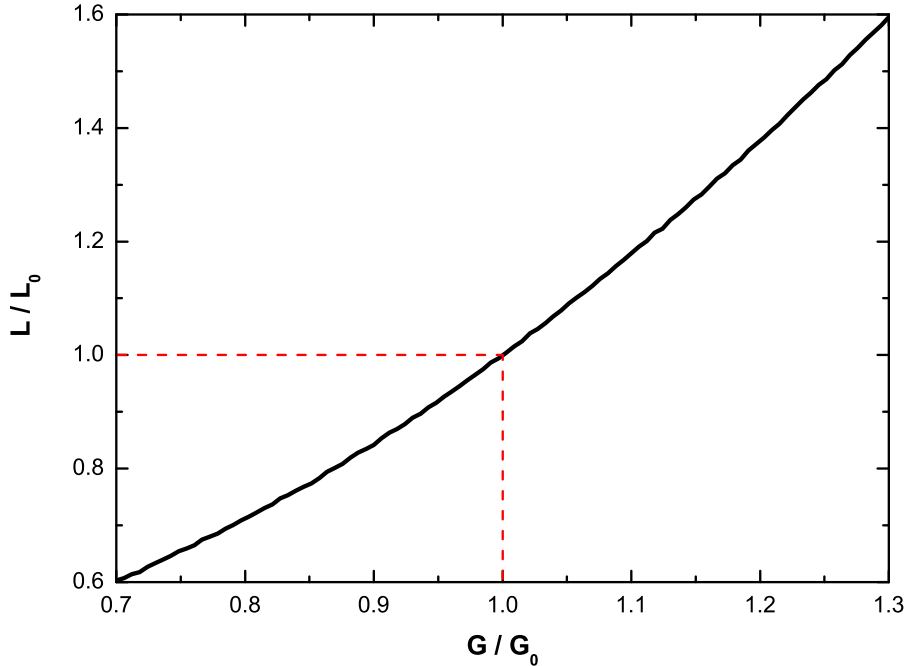
FIG. 1: The calibrated intrinsic luminosity L of SNIa as a function of G, where G_0 is the present-day value, and L_0 is the absolute luminosity of SNIa at $G = G_0$.

where m_{B}^* is the observed peak magnitude in the rest-frame B band, X_1 is a time stretching of the light-curve, and C is a supernova colour at maximum brightness. For any given SNIa, these quantities are obtained from a fit to the light-curve model of SNIa. α and β are the nuisance parameters. The absolute magnitude M_{B} depends on the host galaxy properties, which can be approximately corrected by assuming that M_{B} is related to the host stellar mass through $M_B = M_B^1$ if the host stellar mass is smaller than 10^{10} solar masses while $M_B = M_B^1 + \Delta_M$ if otherwise, where $\Delta_M = -0.08$mag. The absolute magnitude M_B^1 is calibrated for $X_1 = C = 0$ and is treated as a constant [13], relating to the calibrated intrinsic luminosity L as $M_B^1 = M_\odot - 2.5 \log_{10}(L/L_\odot)$, where $M_\odot$ and $L_\odot$ are the Sun's absolute magnitude and luminosity respectively.

In theories of modified gravity with variable G, the M_{B}^1 of SNIa is not a constant. Analytical models of the light curve predict that the peak luminosity of a SNIa is proportional to the mass of nickel synthesised [15], which is approximated to be proportional to the Chandrasekhar mass M_{Ch} [16]. M_{Ch} is the theoretical limit around which an accreting white dwarf will undergo supernova [14]. Since M_{Ch} depends on G, the measurement of peak luminosity of SNIa can be used to determine the variation of G with redshift. In [17], the full effect of a time variation of G on the combined UV+optical+IR SNIa light curves was investigated by a semi-analytic analysis. This method enabled calibration of luminosities based on time-stretching. In this treatment, the main effect is a change of the Chandrasekhar mass, $M_{\mathrm{Ch}} \propto G^{-3/2}$. If G deviates from the its present-day value G_0, M_{Ch} differs from 1.44 solar masses, which leads to the modification of the time-stretch calibrated intrinsic luminosity L. The physics behind why changing M_{Ch} affects the time-stretch calibrated intrinsic luminosity is as follows. A larger M_{Ch} will lead to a larger mass of ejecta in the aftermath of the supernova explosion, which in turn will hinder the transmission of radiation through the ejecta. This results in a fainter, wider light curve. When this light-curve is rescaled to calibrate for the time-stretching, the decrease in width requires a further matching decrease in luminosity. Thus there is a negative relation between M_{Ch} and the time-stretch calibrated intrinsic luminosity L, and since $M_{\mathrm{Ch}} \propto G^{-3/2}$, a positive relationship between G and L. A full discussion of this effect is contained in [17]. The predicted L as a function of G using the analysis of [17] is presented in Fig. 1, which shows a sensitive dependence of L on G. Therefore, if the value of L, or equivalently the M_B^1, can be determined at different redshifts, we could infer the local value of G, which provides a novel method to measure G in different redshift ranges.

III. GW STANDARD SIRENS

From Eq. (1), we observe that for any given SNIa, the value of $M_{\rm B}^1$ can be derived if one can independently measure the luminosity distance $d_{\rm L}$. GW standard sirens provide a model-independent way to achieve this. From the observations of GW signals, caused by coalescence of binary neutron stars (BNSs), one can obtain the $d_{\rm L}$ of a GW event in an absolute way, without having to rely on a cosmic distance ladder [18]. In many cases, it is also possible to identify their electromagnetic counterparts and determine their redshifts [19–21]. Therefore, this provides a novel way to construct the Hubble diagram over a wide redshift range. The third-generation (3G) GW experiments can detect the high-redshift GW signals. By combining the $d_{\rm L}$ and z of standard sirens, we can directly construct the distance modulus as a function of z for a wide redshift range.

Two proposals are currently under consideration for 3G GW detectors: the Einstein Telescope (ET) in Europe [22], and the Cosmic Explorer (CE) in the U.S. [23]. The coordinates and orientations of ET and CE are given in Table 1 of [24], and the amplitude spectral densities are given by Fig. 1 of [24]. ET consists of three Michelson interferometers, and interarm angle of $60°$, arranged to form an equilateral triangle, and we adopt the ET-D configuration in this paper [22]. We consider a 3G network consisting of ET and CE, and summarise the main results as follows. The response of an incoming GW signal is a linear combination of two wave polarisations, $d_I(t) = F_I^+ h_+(t) + F_I^\times h_\times(t)$. The detector's beam-pattern functions F_I^+ and $F_I^\times$ depend on the source localization (θ_s, ϕ_s) and the polarisation angle ψ_s. The restricted post-Newtonian approximated waveforms h_+ and $h_\times$ for the non-spinning BNSs depend on the mass ratio $\eta \equiv m_1 m_2/(m_1+m_2)^2$, the chirp mass $\mathcal{M}_c \equiv (m_1+m_2)\eta^{3/5}$ (m_1 and m_2 are the physical masses of stars), the $d_{\rm L}$, the inclination angle ι, the merging time t_c and merging phase ψ_c [25]. So, for a given BNS, the response of detector depends on $(\mathcal{M}_c, \eta, t_c, \psi_c, \theta_s, \phi_s, \psi_s, \iota, d_{\rm L})$. Employing the nine-parameter Fisher matrix Γ_{ij} and marginalising over the other parameters, we derive the uncertainty $(\Gamma^{-1})_{ii}^{1/2}$ for the i-th parameter in analysis, with $i = 9$ for $d_{\rm L}$ (see [24] for details).

In the low-z range, it is possible to identify the electromagnetic counterparts (e.g., kilonovae [26]) of GW events and fix their redshifts. We numerically simulate the BNS samples with random binary orientations and sky directions. The redshifts are uniformly distributed in comoving volume in the range $z < 0.1$. Current observation of the GW170817 burst predicts the event rate in the range of $[320, 4740]\mathrm{Gpc}^{-3}\mathrm{year}^{-1}$[27]. Assuming three-year observations by a 3G network, we expect to observe $[3.0 \times 10^2, 4.5 \times 10^3]$ events at $z < 0.1$, and $[5.4 \times 10^5, 8.1 \times 10^6]$ events at $z < 2$. We randomly select 1000 samples with $z < 0.1$ to mimic the detections of 3G network in low-z range. In addition, a pessimistic case with 300 events, and an optimistic case with 4500 events are also discussed below for comparison. For each sample, distance measurements include two kinds of uncertainties: the instrumental error $\Delta d_{\rm L}$ calculated above, and an error $\tilde{\Delta} d_{\rm L}$ due to the effects of weak lensing, which can be assumed as $\tilde{\Delta} d_{\rm L}/d_{\rm L} = 0.05z$ [28]. Thus, the total uncertainty is $\sigma_{d_{\rm L}} = [(\Delta d_{\rm L})^2 + (\tilde{\Delta} d_{\rm L})^2]^{1/2}$.

For high-z BNSs, the promising method to measure their redshifts is to observe their short-hard γ-ray burst (shGRB) counterparts. However, the γ radiation is emitted in a narrow cone nearly perpendicular to the binary orbital plane, and the observed shGRBs are nearly all beamed towards the Earth [29]. For these face-on binaries, the parameters $(\theta_s, \phi_s, \iota, \psi_s)$ can be fixed by electromagnetic observations. We repeat the calculation for a large number of face-on GW sources assuming a uniform distribution in comoving volume for a redshift range of $0.1 < z < 2$, as stated above, but adopting a five-parameter Fisher matrix. Although about 10^6 GW events are expected to be observed, only a small partial of them can be treated as standard sirens with measured redshifts. Similar to previous works [24, 28], we conservatively estimate that only 1000 BNSs are used as standard sirens, which are randomly chosen to mimic the observations in high-z range. Fig. 2 presents the redshift distribution and uncertainty of $d_{\rm L}$ for the samples in both low-z and high-z ranges. Note that, we also consider the case with 2000 events for comparison. Following [30], for each BNS, we take the value of $d_{\rm L}$ to be the exact value of a given model, so we expect constraints to be centered on the fiducial parameter values rather than displaced by $\sim 1\sigma$. These constraints can be thought of as the average over many possible realisations of the data.

Note that in some specific modified gravity theories, for instance theories with time-dependent effective Planck mass [31] or non-local modifications [32], the effective luminosity distance of GW could be different from that of electromagnetic waves. Comparison of these two distances provides a novel way to test these gravitational theories [31, 32]. Unlike such previous works, in this paper we consider a phenomenological theory of gravity, which is the same as GR but allowing the value of G to be time-dependent. The waveforms of GW in this theory have been explicitly studied in the literature [33]. Although the definition of $d_{\rm L}$ is the same as in GR, a time-dependent G can generally revise the GW waveform of compact binaries, which could influence the determination of $d_{\rm L}$ from GW observations [33]. However, for the GW events of BNS coalescence observed by 3G network, the duration is typically several minutes, and the variation of G during the GW burst is negligible [33]. Therefore, for each GW event, we can consider G to be constant. For this case, GW waveforms depend on G only through the combination of Gm_1 (or Gm_2) [34], i.e. the NS masses and G value are completely degenerate, and a deviation of G from G_0 cannot influence the determination of $d_{\rm L}$.
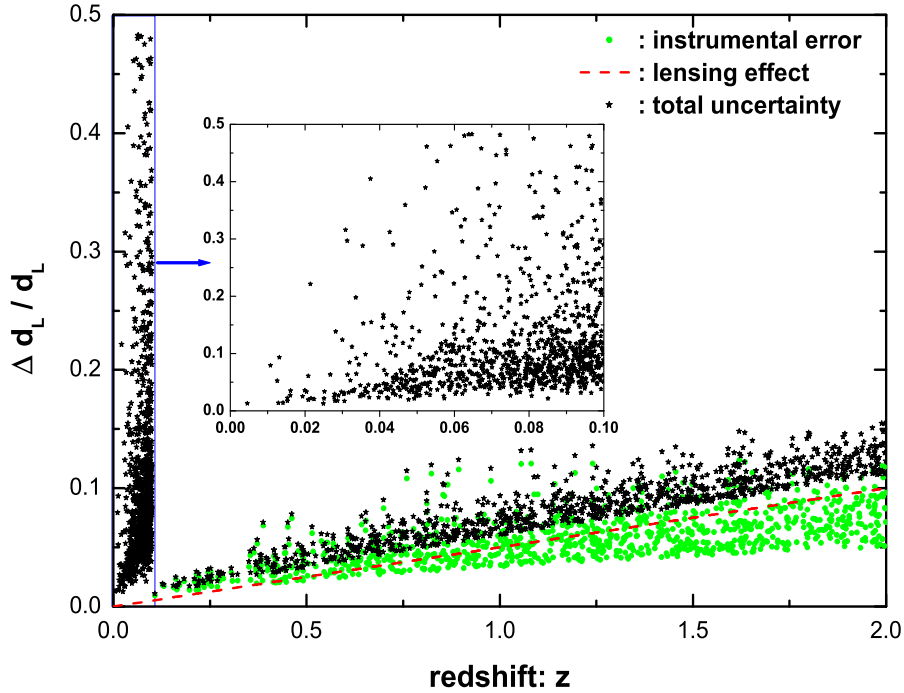
FIG. 2: The values of $\Delta d_{\mathrm{L}}/d_{\mathrm{L}}$ (green dot), $\tilde{\Delta} d_{\mathrm{L}}/d_{\mathrm{L}}$ (red line), $\sigma_{d_{\mathrm{L}}}/d_{\mathrm{L}}$ (black star) for the simulated GW samples, including 1000 BNSs at $z < 0.1$, and 1000 face-on ones at $0.1 < z < 2$. Note that, for the low-z events, we have not presented the results of $\Delta d_{\mathrm{L}}/d_{\mathrm{L}}$, which are overlapped with the corresponding results of $\sigma_{d_{\mathrm{L}}}/d_{\mathrm{L}}$.

IV. MEASURING NEWTON'S CONSTANT

In this paper, the JLA compilation [13] is adopted as an example. Covering a redshift range $0.01 < z < 1.3$, the JLA compilation assembles 740 SNIa samples. To study the evolution of model parameters with redshift, we employ a redshift tomographic method. To be specific, the JLA samples are binned into the following subgroups according to their redshifts: (1) $z < 0.1$; (2) $0.1 < z < 0.2$; (3) $0.1 < z < 0.4$; (4) $0.1 < z < 1.3$; (5) $0.4 < z < 1.3$. In each subgroup, i.e. each redshift range, we assume the value of G, (i.e., M_B^1), is a constant. Also, we assume the relation Eq. (1) holds for each sample. However, the values of the nuisance parameters α and β could be different for different subgroups. Therefore, if the values of M_B^1 at different redshift ranges are obtained, the difference of G between different redshifts can be inferred.

The theoretical values of distance modulus μ strongly depend on the cosmological parameters. To avoid model-dependence in our measurement of the redshift evolution of G, we need an alternative method to determine the value of μ at different redshifts. Future detectable GW events are expected to distribute in nearly the same redshift range as the SNIa data, and the d_{L} of GW events can be determined by the GW observations alone. For each SNIa sample with fixed redshift z, we can derive its distance d_{L} (or distance modulus μ) from nearby GW events by a proper interpolation. When linear interpolation is used, the resulting μ and its error σ_μ at redshift z can be calculated by

$$\mu = \left[\frac{z_{i+1} - z}{z_{i+1} - z_i}\right]\mu_i + \left[\frac{z - z_i}{z_{i+1} - z_i}\right]\mu_{i+1}, \tag{2}$$

$$\sigma_\mu^2 = \left[\frac{z_{i+1} - z}{z_{i+1} - z_i}\right]^2 \sigma_{\mu,i}^2 + \left[\frac{z - z_i}{z_{i+1} - z_i}\right]^2 \sigma_{\mu,i+1}^2, \tag{3}$$

in which μ_i, μ_{i+1} are the distance moduli of the GW events, and $\sigma_{\mu,i}$, $\sigma_{\mu,i+1}$ their errors, at nearby redshifts z_i and z_{i+1}, respectively.
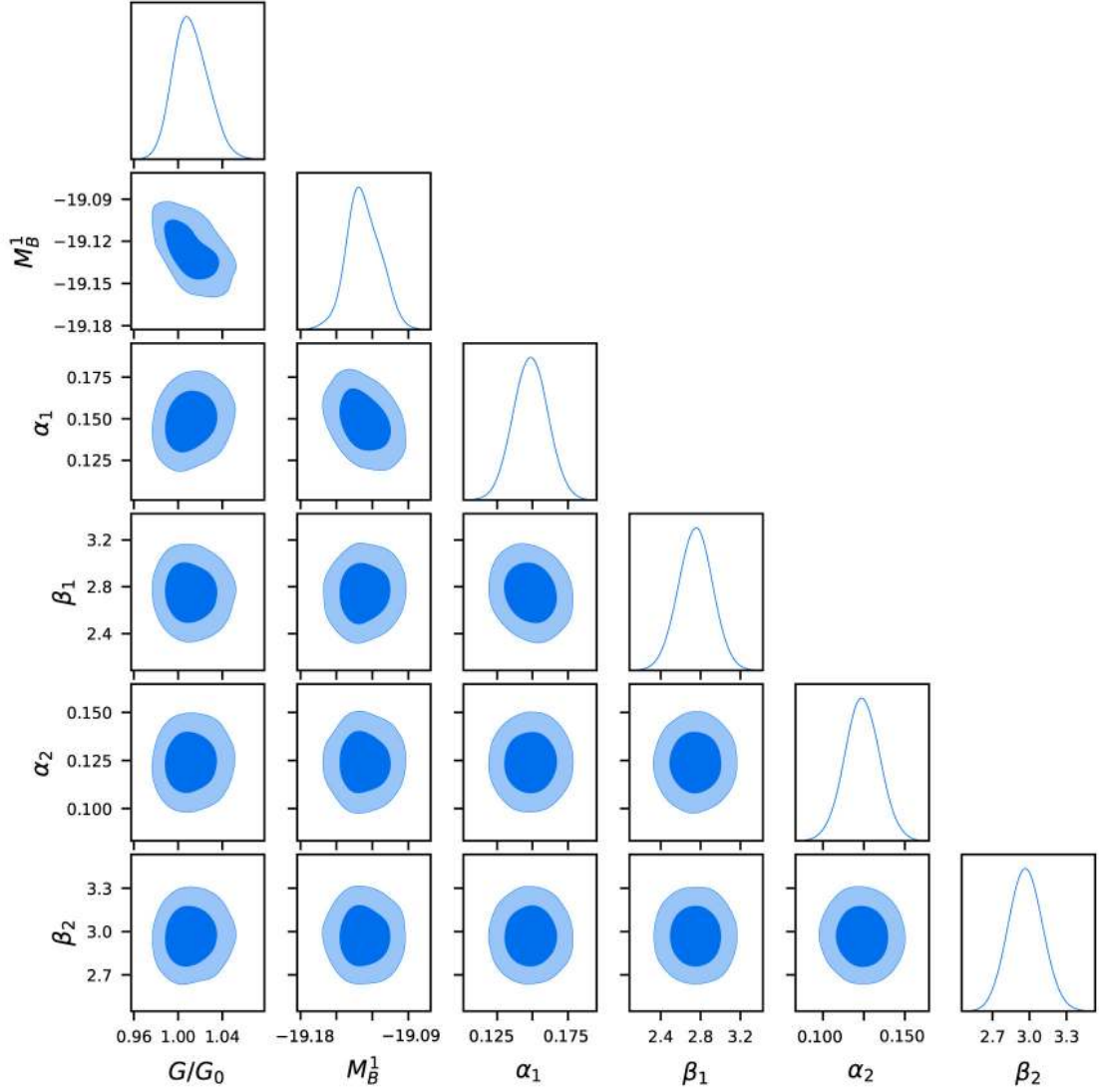
FIG. 3: Two-dimensional and one-dimensional constraint contours for six parameters, where we have considered the case of combining SNIa data at $z < 0.1$ with those at $0.1 < z < 0.2$. The two-dimensional contours denote 1σ and 2σ constraints, respectively.

We first investigate the possible difference of G in the redshift ranges $z < 0.1$ and $0.1 < z < 0.2$. Considering the SNIa samples of these two subgroups, for each SNIa, z is known, μ and σ_μ are derived from the interpolation of GW data, and the values of $m_{\rm B}^*$, X_1 and C are given in [13]. For these data in two bins, we have six parameters ($M_{\rm B}^1$, α_1, β_1, G/G_0, α_2, β_2), where (α_1, β_1) and (α_2, β_2) are the nuisance parameters in the first and second redshift bin, respectively, $M_{\rm B}^1$ is the calibrated absolute magnitude of SNIa at $z < 0.1$, and G_0, G are the Newton's constant in the two redshift bins. Note that, throughout this paper we assume G_0, the value in the first z-bin, is equal to the G value today, and that the calibrated absolute magnitude of SNIa in the second bin has been expressed by $M_{\rm B}^1$ and G/G_0. We apply the following χ^2 calculation to obtain the constraints on six parameters,

$$
\begin{aligned}
\chi^2 = & \sum_i \frac{[\mu^{(i)} - (m_{\rm B}^* - M_{\rm B} + \alpha X_1 - \beta C)^{(i)}]^2}{\sigma_{\mu^{(i)}}^2 + \sigma_{(m_{\rm B}^* - M_{\rm B} + \alpha X_1 - \beta C)^{(i)}}^2 + \sigma_{s^{(i)}}^2} \\
& + \sum_j \frac{[\mu^{(j)} - (m_{\rm B}^* - M_{\rm B} + \alpha X_1 - \beta C)^{(j)}]^2}{\sigma_{\mu^{(j)}}^2 + \sigma_{(m_{\rm B}^* - M_{\rm B} + \alpha X_1 - \beta C)^{(j)}}^2 + \sigma_{s^{(j)}}^2},
\end{aligned}
\tag{4}
$$

TABLE I: The uncertainties of six parameters for SNIa in different redshift bins combined with those in $z < 0.1$.

	$0.1 < z < 0.2$	$0.1 < z < 0.4$	$0.1 < z < 1.3$	$0.4 < z < 1.3$
G/G_0	1.011 ± 0.016	1.010 ± 0.015	1.007 ± 0.015	0.997 ± 0.016
M_{B}^1	-19.13 ± 0.01	-19.13 ± 0.01	-19.13 ± 0.01	-19.12 ± 0.01
α_1	0.149 ± 0.012	0.149 ± 0.012	0.149 ± 0.012	0.149 ± 0.012
β_1	2.744 ± 0.170	2.749 ± 0.170	2.747 ± 0.169	2.747 ± 0.170
α_2	0.124 ± 0.010	0.140 ± 0.008	0.136 ± 0.007	0.119 ± 0.016
β_2	2.972 ± 0.139	3.037 ± 0.100	2.953 ± 0.083	2.738 ± 0.161

where i and j indicate the SNIa samples in first and second redshift bin respectively, and $\sigma_s^2 = (5\sigma_z/z \log 10)^2 + \sigma_{\mathrm{lens}}^2 + \sigma_{\mathrm{coh}}^2$, which accounts for the uncertainty in cosmological redshift due to peculiar velocity, the variation of magnitudes caused by gravitational lensing, and the intrinsic variation in SN magnitude not described by other terms [13]. We use $c\sigma_z = 150 \mathrm{km/s}$ and $\sigma_{\mathrm{lens}} = 0.055z$ as suggested in [13, 35]. The values of σ_{coh} are adopted as in [13]. Note that, in this calculation, we have ignored the weak correlation between different SNIa data, which only slightly changes the uncertainties of the constrained parameters.

Employing a modified CosmoMC package [36], we obtain the marginalised constraints on each parameter, which are listed in Table I, and the one-dimensional likelihood functions and two-dimensional contours are presented in Fig. 3. To measure the value of G in different redshift ranges, we replace the second redshift bin $0.1 < z < 0.2$ with that in $0.1 < z < 0.4$, $0.1 < z < 1.3$, $0.4 < z < 1.3$, respectively. The corresponding constraints are also presented in Table I. We find that for each case, the uncertainty of G/G_0 is ~ 0.015. These results show that, by combining the SNIa data and potential 3G GW data, the deviation of Newton's constant from G_0 at high redshifts can be expected to be constrained at 1.5% level. The uncertainty in G/G_0 is mainly caused by the error bars of μ in the first redshift bin, which in turn are determined by the errors on d_{L} for GW events in the same redshift range. For comparison, we keep the second redshift bin as $0.1 < z < 0.2$, and change the first bin to $z < 0.03$, $z < 0.05$ and $0.05 < z < 0.1$. The corresponding uncertainties of G/G_0 become 0.018, 0.017, 0.022 respectively, which are larger than 0.015 as anticipated.

Note that the number of observable GW events, N_{GW}, is quite uncertain. In order to test how the uncertainty of G/G_0 depends on N_{GW}, we compare the following cases: (1) 1000 low-z and 1000 high-z GW events as above; (2) 300 low-z and 1000 high-z GW events; (3) 4500 low-z and 1000 high-z GW events; (4) 1000 low-z and 2000 high-z GW events. For each case, we consider the SNIa samples in two bins ($z < 0.1$ and $0.1 < z < 0.2$), and derive the constraints of six parameters by a similar analysis as above. We find that the results are nearly the same in all cases, which is understandable: the GW observations influence our results only through Eqs. (2) and (3), and these two relations show that the values of μ and σ_μ for each SNIa depend only on its nearby GW events, and increasing or decreasing N_{GW} cannot significantly affect their values. Of course, if the redshift distribution of GW events is too sparse, i.e. N_{GW} is too small, the interpolation in Eqs. (2) and (3) is not applicable any more, and the derived constraints on G/G_0 become unreliable. Therefore, to keep the stability of the results, the number of GW events should be comparable to, or even larger than, that of SNIa in the corresponding redshift ranges.

V. CONCLUSIONS

The calibrated intrinsic peak luminosity of a SNIa depends on the strength of gravity in the supernova's local environment. If d_{L} can be determined by independent observations, the SNIa can be treated as a tracker to measure the variation of gravitational constant G in a wide redshift range. We propose to use the GW standard sirens distributed in a similar redshift range to determine d_{L} of SNIa by interpolation. As an application, we consider the recent JLA compilation of SNIa data, for which d_{L} values are assumed to be determined 3G GW observations. Splitting the SNIa samples into several subgroups according to their redshifts, we determine the value of G in different redshift ranges. We find that the ratio G/G_0, where G is the gravitational constant in the redshift $z > 0.1$ and G_0 is that at $z_0 < 0.1$, can be determined at the level of 1.5%.

As examples to compare our results with other constraints, we adopt $z = 0.4$ ($z = 0.9$) and assume a power-law cosmic time dependence, $G \propto t^{-\alpha}$, then the constraint $\Delta G(z)/G < 0.015$ is equivalent to a constraint on the index of $|\alpha| \lesssim 0.04$ (0.02), which can be translated into $|(\mathrm{d}G/\mathrm{d}t)/G|_{t=t_0} \lesssim 3 \times 10^{-12}$ year^{-1} (1.5×10^{-12} year^{-1}). This is of the same order as constraints from pulsars [4], lunar laser ranging [3] and BBN [5] ($|(\mathrm{d}G/\mathrm{d}t)/G|_{t=t_0} \lesssim 10^{-12}$ year^{-1}). Most importantly, the new method offers a novel and independent way to constrain Newton's constant G over a wide redshift range $0 < z < 1.3$, which could also be extended to $0 < z < 2$ by future SNIa observations [37].

Acknowledgments

[1] S. Weinberg, Gravitation and Cosmology, (John Wiley & Sons, Inc, 1972).
[2] X. Zhang, W. Zhao, H. Huang and Y. F. Cai, Phys. Rev. D **93**, 124003 (2016).
[3] J. G. Williams, S. G. Turyshev and D. H. Boggs, Phys. Rev. Lett. **93**, 261101 (2004).
[4] V. M. Kaspi, J. H. Taylor and M. F. Ryba, ApJ **428**, 713 (1994); W. W. Zhu, G. Desvignes, N. Wex et al., arXiv:1802.09206.
[5] C. J. Copi, A. N. Davis and L. M. Krauss, Phys. Rev. Lett. **92**, 171301 (2004); R. H. Cyburt, B. D. Fields, K. A. Olive and E. Skillman, Astropart. Phys. **23**, 313 (2005).
[6] E. Garcia-Berro, J. Isern and Y. A. Kubyshin, Asron. Astrophysics Rev. **14**, 113 (2007).
[7] J. P. Uzan, Living Rev. Relativity **14**, 2 (2011).
[8] W. Hillebrandt and J. C. Niemeyer, ARA&A **38**, 191 (2000).
[9] E. Garcia-Berro, Y. A. Kubyshin, P. Loren-Aguilar and J. Isern, IJMPD **15**, 1163 (2006).
[10] J. Mould and S. A. Uddin, PASA **31**, 5 (2014).
[11] M. M. Phillipse, ApJ, **413**, L105 (1993).
[12] S. Weinberg, Cosmology, (Oxford University Press, New York, 2008).
[13] M. Betoule, et al., A&A **568**, A22 (2014).
[14] S. Chandrasekhar, ApJ, **74**, 81 (1931).
[15] D. Arnett, ApJ **253**, 785 (1982).
[16] E. Gaztanaga, E. Garcia-berro, J. Isern, E. Bravo and I. Dominguez, Phys. Rev. D **65**, 023506 (2001).
[17] B. S. Wright and B. Li, Phys. Rev. D **97**, 083505 (2018).
[18] B. F. Schutz, Nature (London) **323**, 310 (1986); LIGO Scientific and Virgo Collaboration, Nature (London), **551**, 85 (2017).
[19] B. P. Abbott et al., Phys. Rev. D **93**, 122008 (2016); ApJ **841**, 89 (2017).
[20] LIGO Scientific Collaboration et al., ApJ **848**, L12 (2017).
[21] D. A. Coulter, R. J. Foley, C. D. Kilpatrick, M. R. Drout et al., Science **358**, 1556 (2017).
[22] http://www.et.et-gw.eu/.
[23] B. P. Abbott et al., Class. Quantum Gravity **27**, 084007 (2010).
[24] W. Zhao and L. Wen, Phys. Rev. D **97**, 064031 (2018).
[25] B. S. Sathyaprakash and B. Schutz, Living Reviews in Relativity **12**, 2 (2009).
[26] P. A. Evans et al., Science **358**, 1565 (2017).
[27] LIGO Scientific Collaboration and Virgo Collaboration, Phys. Rev. Lett. **119**, 161101 (2017).
[28] B. S. Sathyaprakash, B. Schutz and C. Van Den Broeck, Class. Quantum Gravity **27**, 215006 (2010); W. Zhao, C. Van Den Broeck, D. Baskaran and T. G. F. Li, Phys. Rev. D **83**, 023005 (2011).
[29] T. Piran, Phys. Rep. **333**, 529 (2000); E. Nakar, Phys. Rep. **442**, 166 (2007).
[30] M. J. Mortonson and W. Hu, Phys. Rev D **77**, 043506 (2008).
[31] L. Amendola, I. Sawicki, M. Kunz and I. D. Saltas, JCAP **08**, 030 (2018).
[32] E. Belgacem, Y. Cirian, S. Foffa and M. Maggiore, Phys. Rev. D **97**, 104066 (2018).
[33] N. Yunes, F. Pretorius and D. Spergel, Phys. Rev. D **81** 064018 (2010).
[34] M. Maggiore, Gravitational Waves, (Oxford University Press, New York, 2008).
[35] J. Jonsson et al., MNRAS **405**, 535 (2010).
[36] A. Lewis and S. Bridle, Phys. Rev. D **66**, 103511 (2002).
[37] Z. Ivezic et al., arXiv:0805.2366; R. Hounsell et al., arXiv:1702.01747.